PHYSICAL REVIEW B **71**, 125208 (2005)

Analysis of the steady-state photocarrier grating method for the determination of the density of states in semiconductors

J. A. Schmidt

INTEC (UNL-CONICET), Güemes 3450, 3000 Santa Fe, Argentina,
and FIQ (UNL), Santiago del Estero 2829, 3000 Santa Fe, Argentina

C. Longeaud

Laboratoire de Génie Electrique de Paris, (UMR 8507 CNRS) Ecole Supérieure d'Electricité, Universités Paris VI et XI,
Plateau de Moulon, 91192 Gif-sur-Yvette CEDEX, France

(Received 16 June 2004; revised manuscript received 4 January 2005; published 18 March 2005)

In this paper we present a complete theoretical analysis of the steady-state photocarrier grating (SSPG) method, starting from the generalized equations that describe charge transport and recombination under grating conditions. The analytical solution of these equations and the application of simplifying assumptions leads to a very simple formula relating the density of states (DOS) at the quasi-Fermi level for trapped electrons to the SSPG signal at large grating periods. By means of numerical calculations reproducing the experimental SSPG curves we test our method for DOS determination. We examine previous theoretical descriptions of the SSPG experiment, illustrating the case when measurements are performed at different illumination intensities. We propose a procedure to estimate the minority-carriers mobility-lifetime product from SSPG curves, introducing a correction to the commonly applied formula. We illustrate the usefulness of our technique for determining the DOS in the gap of intrinsic semiconductors, and we underline its limitations when applied to hydrogenated amorphous silicon. We propose an experimental procedure that improves the accuracy of the SSPG-DOS reconstruction. Finally, we test experimentally this new method by comparing the DOS obtained from SSPG and modulated photocurrent measurements performed on the same samples. The experimental DOS obtained from both methods are in very good agreement.

DOI: 10.1103/PhysRevB.71.125208 PACS number(s): 73.50.Pz, 72.20.Jv, 73.61.Jc

I. INTRODUCTION

The localized states in the gap of amorphous semiconductors determine the transport properties of these materials, so a detailed knowledge of the density of states (DOS) within the energy gap is of great interest. Several methods have been proposed to probe the DOS as a function of energy, like field-effect,[1] space-charge-limited currents,[2] capacitance,[3] transient photocurrent,[4] photoemission,[5] time of flight,[6] optical absorption,[7] thermally stimulated conductivity,[8,9] modulated photoconductivity in the high frequency[10] and low frequency[11] regimes, and steady-state photoconductivity.[12,13] The methods used to estimate the DOS can be divided into two categories: (i) methods where an initial DOS described by several parameters is proposed, obtaining the parameter values from a fit of the experimental data with the results of numerical calculations resulting from a theoretical description of the experiment; (ii) methods where the experimental data are used directly to determine the DOS, based on a reconstruction formula derived from the theoretical analysis of the experiment. The drawback of the methods belonging to the first category is that no less than twenty parameters are involved in the description of the DOS, so the uniqueness of the fit cannot be ensured—even when a single set of parameter values is used to fit the results of several measurements. The main drawback of the second group of methods is that the DOS is only obtained over a limited energy range. In a recent publication[14] the authors presented a new method belonging to the second category, based on steady-state photocurrent grating (SSPG) measurements. In this work we discuss the method in more detail, presenting new experimental results for hydrogenated amorphous silicon samples.

The SSPG technique was introduced in 1986 by Ritter, Zeldov and Weiser[15] as a method (hereafter referred as the RZW method) to measure the ambipolar diffusion length (L_{amb}) of low-mobility semiconductors. The technique became a standard method for material characterization in several laboratories, and it was applied not only to amorphous silicon and its alloys[16–18] but also to microcrystalline silicon[19,20] and to crystalline materials.[16,21] Several authors analyzed different aspects of the SSPG method, contributing to an understanding of the physics involved. In their original treatment, Ritter, Zeldov and Weiser presented a simple formula to obtain L_{amb} under the assumption of ambipolar transport and space-charge neutrality.[15,16] The same authors performed later a more detailed analysis of the method, numerically solving the transport equations in the small-signal approximation.[22] They established the limits of validity of the simple formula to get L_{amb} from SSPG measurements, namely under low applied electric fields and in the "lifetime regime," a regime where the dielectric relaxation time τ_d is much smaller than the carrier lifetimes. In 1990, Balberg[23] obtained analytical solutions for the transport equations in the limit of a low applied electric field, thus further clarifying the conditions that allow an interpretation of the experimental results in terms of L_{amb}. Later, Li[24] and Balberg[25] solved independently the transport equations under the influence of an externally applied electric field, obtaining

 ©2005 The American Physical Society

analytical solutions in the regions of low and high fields. Hattori and co-workers[26] used a second-order perturbation approach to solve the SSPG transport equations in the small-signal approximation, revealing deficiencies of the previous analyses. These authors studied the light-intensity dependence of the transport parameters, and they proposed a method to correct the apparent diffusion length that is obtained when the RZW formula is used to treat the data.

Most of the previously mentioned analyses of the SSPG method described the transport equations based on the concept of drift or trap-limited mobilities and a phenomenologically introduced recombination lifetime, treating the photocarriers (free plus trapped) as a whole. On the other hand, Abel and Bauer[27] based their description of the SSPG experiment on the free carriers concentration and their extended-states mobility-lifetime products. These authors presented a generalized theory of the SSPG leading to an analytical expression capable of fitting experiments in which the external electric field and the period of the photocarrier grating are varied simultaneously. At the same time, these authors implemented numerical simulations to validate their analytical expressions, and they applied their method to measurements performed on hydrogenated amorphous silicon (a-Si:H) samples. In spite of their great contribution to the understanding of the SSPG method, Abel and Bauer treated the carriers recombination phenomenologically, without specifying the microscopic mechanisms. For that reason, the density of recombination centers does not appear in their formulation.

Finally, Balberg and co-workers applied the SSPG method in conjunction with steady-state photoconductivity to estimate the DOS of amorphous[28,29] and microcrystalline silicon.[30] The procedure used by these authors consisted on fitting the temperature dependence of four phototransport properties (namely, the two carriers mobility-lifetime products and their light intensity exponents) with the results of computer simulations arising from a pre-suggested DOS. Thus, this method belongs to the first category mentioned above. To our knowledge, no attempts to derive the density of localized states directly from the application of a reconstruction formula to SSPG measurements had been presented until our recent paper.[14]

This work is organized as follows. In Sec. II we present the basic equations describing the SSPG experiment and we solve them analytically to obtain a generalized expression for the current density under grating conditions. Then we find simplified expressions applicable in general to intrinsic semiconductors, and we propose further simplifications valid for a-Si:H. Finally, we go to the limit of large grating periods, showing that the DOS at the quasi-Fermi energy can be obtained from a very simple formula. In Sec. III we verify the validity of the simplifying assumptions and of the final theoretical expression from the results of numerical simulations. We examine the accuracy of previous theoretical analyses of the SSPG experiment, and we propose a correction procedure to the RZW formula[16] to get the right value for the minority carriers mobility-lifetime product. We study the limitations of our method and the range of experimental conditions that ensure its validity, proposing the best experimental conditions under which the method should be applied. In Sec. IV we prove the applicability of this new method by performing measurements on a-Si:H samples. We compare the results of the new method with measurements performed by using the modulated photocurrent methods, showing the good agreement between the DOS determinations. Finally, we conclude in Sec. V.

II. THEORY

A. Basic equations

The SSPG experiment is usually performed by illuminating the sample with a steady laser beam of high intensity and a less intense beam chopped at a pulsation ω. The case when ω is increased to a value comparable to the inverse of the carriers lifetime has been treated in a recent paper by Nicholson.[31] In the following, however, we will assume $\omega=0$; an assumption that does not alter the following treatment since ω is usually chosen very small. When the two laser beams of intensities I_1 and I_2 interfere on the sample surface (coordinate x), an intensity grating $I(x)=I_1+I_2+\gamma_0 2\sqrt{I_1 I_2}\cos(2\pi x/\Lambda)$ is created, where the grating period is $\Lambda=\lambda/[2\sin(\delta/2)]$, λ being the laser wavelength and δ the angle between the two beams. The factor γ_0, which takes values between zero and one, accounts for the grating quality due to partial coherence of the beams, mechanical vibrations or light scattering.[16,20] The nonuniform illumination leads to a spatially modulated generation rate, $G(x)=G_0+\Delta G\cos(kx)=G_0+\Re e[\Delta G e^{jkx}]$, $k=2\pi/\Lambda$, $j^2=-1$, and $\Re e$ meaning the real part of the complex number. This spatially modulated generation rate in turn creates free electrons and holes distributions, $n(x)$ and $p(x)$, with the same period. However, since electrons and holes have different diffusion coefficients, the amplitudes and phases of the two distributions will differ, generating an internal electric field, $\xi_{\text{int}}(x)$, that will add to the externally applied electric field ξ_{ext}. The internal electric field is related to the local charge densities via Poisson's equation,

$$\frac{d\xi_{\text{int}}(x)}{dx}=\frac{q}{\varepsilon\varepsilon_0}\left\{p(x)+\int_{E_v}^{E_c}[1-f(E,x)]N^{DON}(E)dE-n(x)-\int_{E_v}^{E_c}f(E,x)N^{ACC}(E)dE\right\}, \quad (1)$$

where ε is the dielectric constant of the sample, ε_0 is the dielectric permittivity of vacuum, E_v is the energy at the top of the valence band, E_c is the energy at the bottom of the conduction band, $f(E,x)$ is the occupation function, $N^{DON}(E)$ is the density of donor states (neutral when occupied and positively charged when empty), and $N^{ACC}(E)$ is the density of acceptor states (neutral when empty and negatively charged when occupied). Though we have solved analytically the equations describing the SSPG experiment for a DOS made of different types of states (monovalent and/or amphoteric), for clarity we will concentrate here on a single type of monovalent states.

Both the externally applied electric field and the internally developed space charge field will contribute to the current

density under coherent illumination, which is given by

$$j_{coh} = \frac{1}{\Lambda}\int_0^{\Lambda} [q\mu_n n(x) + q\mu_p p(x)][\xi_{ext} + \xi_{\rm int}(x)]dx = j_0 + \Delta j. \tag{2}$$

The carrier concentrations $n(x)$ and $p(x)$ are obtained by solving the continuity equations for electrons and holes, which in the steady-state are

$$G(x) - R_n(x) = -\mu_n \frac{d}{dx}[n(x)\xi(x)] - D_n \frac{d^2 n(x)}{dx^2}, \tag{3}$$

$$G(x) - R_p(x) = \mu_p \frac{d}{dx}[p(x)\xi(x)] - D_p \frac{d^2 p(x)}{dx^2}, \tag{4}$$

where μ is the extended-states mobility and D is the diffusion coefficient. Subscripts (n or p) refer to electrons or holes, respectively. The recombination rates $R(x)$ are given by

$$R_n(x) = \int_{E_v}^{E_c} \{c_n n(x)[1 - f(E,x)] - e_n(E) f(E,x)\} N(E) dE, \tag{5}$$

$$R_p(x) = \int_{E_v}^{E_c} \{c_p p(x) f(E,x) - e_p(E)[1 - f(E,x)]\} N(E) dE, \tag{6}$$

where c is the capture coefficient, $e(E)$ is the emission rate, and $N(E)$ is the DOS.

In the low-modulation condition established when $I_1 \gg I_2$, it is expected that the relevant physical parameters vary sinusoidally as $G(x)$ does. In general, however, there will be variable phase shifts, and any quantity can be expressed as $Q(x) = Q_0 + \Re e[\Delta Q e^{jkx}]$, where Q_0 is the value under uniform illumination G_0, and ΔQ originates from the spatially modulated term of the generation rate $\Delta G(x)$. ΔQ can also be written as $\Delta Q = \Delta Q_r + j\Delta Q_i$, the indexes r and i standing for real and imaginary, respectively. This linearizes the system of coupled differential equations (1) and (3)–(6), giving rise to the following system of linear equations:

$$\begin{aligned} &A_n \times \Delta n_r - B_n \times \Delta n_i + A_p^* \times \Delta p_r = \Delta G, \\ &B_n \times \Delta n_r + A_n \times \Delta n_i + A_p^* \times \Delta p_i = 0, \\ &A_n^* \times \Delta n_r + A_p \times \Delta p_r - B_p \times \Delta p_i = \Delta G, \\ &A_n^* \times \Delta n_i + B_p \times \Delta p_r + A_p \times \Delta p_i = 0. \end{aligned} \tag{7}$$

The coefficients are given by

$$A_n = c_n \int [1 - (c_n n_0 + e_n)\tau](1 - f_0) N\, dE + \frac{q\mu_n n_0}{\varepsilon\varepsilon_0} \times \left[1 + c_n \int (1 - f_0)\tau N dE\right] + k^2 D_n,$$

$$A_n^* = c_n \int (c_p p_0 + e_p)\tau(1 - f_0) N\, dE - \frac{q\mu_p p_0}{\varepsilon\varepsilon_0} \times \left[1 + c_n \int (1 - f_0)\tau N dE\right],$$

$$A_p = c_p \int [1 - (c_p p_0 + e_p)\tau] f_0 N\, dE + \frac{q\mu_p p_0}{\varepsilon\varepsilon_0} \times \left[1 + c_p \int f_0 \tau N dE\right] + k^2 D_p,$$

$$A_p^* = c_p \int (c_n n_0 + e_n)\tau f_0 N\, dE - \frac{q\mu_n n_0}{\varepsilon\varepsilon_0} \times \left[1 + c_p \int f_0 \tau N dE\right],$$

$$B_n = -k\mu_n \xi_{ext}, \quad \text{and } B_p = k\mu_p \xi_{ext},$$

where the energy dependence has been omitted for the sake of clarity. Integrals are evaluated between E_v and E_c, and we call $\tau^{-1} = c_n n_0 + c_p p_0 + e_n + e_p$.

From the solution of Eq. (7), analytical expressions for $n(x)$, $p(x)$, and $\xi_{\rm int}(x)$ can be obtained. Inserting them into Eq. (2), it is found that

$$\Delta j(\Lambda) = \frac{q^2(\Delta n_i\, \Delta p_r - \Delta n_r\, \Delta p_i)}{2k\varepsilon\varepsilon_0} \left\{ \mu_n\left[1 + c_p \int f_0 \tau N dE\right] + \mu_n \left[1 + c_p \int (1 - f_0)\tau N dE\right] \right\}. \tag{8}$$

The full expression of $\Delta n_i \Delta p_r - \Delta n_r \Delta p_i$ is rather complex,

$$\Delta n_i \Delta p_r - \Delta n_r \Delta p_i = \frac{\Delta G^2}{DEN}[(A_n - A_n^*) \times B_p - (A_p - A_p^*) \times B_n], \tag{9}$$

where $\Delta G = \gamma_0^2 \sqrt{G_1 G_2}$, G_1 and G_2 being the generation rates originating from I_1 and I_2, respectively, and

$$DEN = [A_n A_p - A_n^* A_p^* - B_n B_p]^2 + [B_n A_p + B_p A_n]^2. \tag{10}$$

B. Simplified expressions

The first simplifications that can be done concern the integrals estimate. These integrals should be calculated over the whole energy gap from E_v to E_c. However, if the DOS function does not vary faster than the Boltzmann factor $e^{E/k_B T}$ (where k_B is Boltzmann's constant and T is the absolute temperature), the exponential variation of the emission rates allows us to restrict the energy range to the $[E_{tp}, E_{tn}]$ interval, E_{tp} and E_{tn} being the quasi-Fermi levels for trapped holes and electrons, respectively, which are fixed by the dc illumination. For instance, in the expression of A_n appears the integral

$$c_n\int_{E_v}^{E_c}(1-f_0)\tau N\,dE = c_nc_pp_0\int_{E_v}^{E_c}\tau^2N\,dE + c_n\int_{E_v}^{E_c}e_n\tau^2N\,dE \approx \tau_t\left[c_nc_pp_0\tau_t\int_{E_{tp}}^{E_{tn}}N\,dE + c_nN_n\right] \approx \tau_t\left[\frac{1}{\tau_n}+c_nN_n\right], \quad (11)$$

where τ_t is defined by $\tau_t=1/(c_nn_0+c_pp_0)$ and $N_n=k_BTN(E_{tn})$, $N(E_{tn})$ being the density of states at the quasi-Fermi level for trapped electrons. τ_n (τ_p) is the free electron (hole) lifetime, defined for steady-state uniform illumination as $\tau_n=(n_0-n_{th})/G_0$ [or, equivalently, $\tau_p=(p_0-p_{th})/G_0$], n_{th} (p_{th}) being the thermal equilibrium electron (hole) density. For insulators or intrinsic semiconductors in the high-generation regime $n_0 \gg n_{th}$ and $p_0 \gg p_{th}$, so from Eq. (15) in Ref. 32 we have

$$\frac{1}{\tau_n}=c_nc_pp_0\tau_t\int_{E_{tp}}^{E_{tn}}N\,dE, \quad \frac{1}{\tau_p}=c_pc_nn_0\tau_t\int_{E_{tp}}^{E_{tn}}N\,dE. \quad (12)$$

We will also call $N_p=k_BTN(E_{tp})$, $N(E_{tp})$ being the density of states at the quasi-Fermi level for trapped holes. The factors N_n and N_p arise from the sharp peaked functions $e_n\tau^2$ and $e_p\tau^2$, centered at E_{tn} and E_{tp}, which can be approximated by Dirac δ functions provided that $N(E)$ does not vary with energy faster than the emission coefficients.

The second approximation that can be done is to neglect the 1 in the expressions $\lfloor 1+c_p\int f_0\tau NdE\rfloor$ and $\lfloor 1-c_n\int(1-f_0)\tau NdE\rfloor$. Indeed, a rapid estimate of these expressions, taking the case of a-Si:H and using the above approximations, shows that the terms containing the integrals are much higher than unity. Actually, both expressions come from Eq. (1), where the "ones" express the contribution of free carriers to the charge neutrality while the integrals express the gap states contribution. Neglecting the "ones" simply means assuming that charge neutrality is mainly controlled by the deep states and not by the free carriers, which must be the case in defective semiconductors.

Using these approximations we will first simplify Eq. (9), before giving a final approximate expression for $\Delta j(\Lambda)$. If we call $X_n=c_n\tau_nN_n$ and $X_p=c_p\tau_pN_p$, Eq. (9) transforms into

$$\Delta n_i\Delta p_r - \Delta n_r\Delta p_i = -\frac{\Delta G^2k\xi_{ext}}{DEN\times\tau_n\tau_p}\left\{\left[\frac{\tau_t}{\tau_d}(1+X_n)+k^2L_n^2\right]\mu_p\tau_p + \left[\frac{\tau_t}{\tau_d}(1+X_p)+k^2L_p^2\right]\mu_n\tau_n\right\}, \quad (13)$$

where $L_n^2=D_n\tau_n$, $L_p^2=D_p\tau_p$, and τ_d is the dielectric relaxation time, given by

$$\frac{1}{\tau_d}=\frac{q(\mu_nn_0+\mu_pp_0)}{\varepsilon\varepsilon_0}=\frac{q}{\varepsilon\varepsilon_0}(\mu_n\tau_n+\mu_p\tau_p)G_0. \quad (14)$$

The expression of DEN is rather long, since, if we write $DEN=A^2+B^2$, we obtain

$$A^2=\left[\begin{array}{c} c_pp_0\frac{\tau_t}{\tau_p}\left(\frac{1}{\tau_n}+c_nN_n+c_nN_p\right)\left(\frac{\tau_t}{\tau_d}(1+X_p)+k^2L_p^2\right) \\ +c_nn_0\frac{\tau_t}{\tau_n}\left(\frac{1}{\tau_p}+c_pN_p+c_pN_n\right)\left(\frac{\tau_t}{\tau_d}(1+X_n)+k^2L_n^2\right) \\ +\mu_n\mu_pK\left(\frac{\tau_t(2+X_n+X_p)}{\tau_d(\mu_n\tau_n+\mu_p\tau_p)}+K\right)+k^2\mu_n\mu_p\xi_{ext}^2 \end{array}\right]^2 \quad (15)$$

and

$$B^2=k^2\xi_{ext}^2\left[\begin{array}{c} -\mu_p\left[c_pp_0\tau_t\left(\frac{1}{\tau_n}+c_nN_n+c_nN_p\right)+\mu_n\frac{q\tau_t}{\varepsilon\varepsilon_0}\frac{n_0}{\tau_n}(1+X_n)+k^2D_n\right] \\ +\mu_n\left[c_nn_0\tau_t\left(\frac{1}{\tau_p}+c_pN_n+c_pN_p\right)+\mu_p\frac{q\tau_t}{\varepsilon\varepsilon_0}\frac{p_0}{\tau_p}(1+X_p)+k^2D_p\right] \end{array}\right]^2, \quad (16)$$

where we call $K=k^2k_BT/q$.

The complete expression of the denominator can be simplified applying some approximations already introduced by other groups.[23–27] First, we will assume that the experiment is performed in the "low electric field" regime. The definition of this regime varies from one author to another, so we will try to clarify this concept. For instance, Abel *et al.*[27] do not explicitly specify the limit between "high electric field" and "low electric field" domains, but the various curves presented in their work [Fig. 6(b) of Philos. Mag. B, Ref. 27] allows us to estimate that the "low electric field" domain comprises fields lower than or equal to 200 V/cm. Li gives a condition [Eq. (54) of Ref. 24] from which, assuming for the case of a-Si:H a ratio of ten between electron and hole mobilities and a diffusion length of the order of 150 nm, one obtains $\xi_{ext} \leq 1000$ V/cm at room temperature. Balberg[25] and Hattori *et al.*[26] propose another expression for the low electric field limit that, at room temperature and for a grating period of 1 μm, gives the condition $\xi_{ext} \leq 1600$ V/cm. Clearly, the definition of the "weak field regime" is not strict and depends on experimental conditions such as temperature, generation rate, and grating period. Note that Hattori *et al.*

have shown that the weak field condition was "intimately correlated with the transition between the lifetime and the relaxation time regimes in the presence of an externally applied field,"[26] so that there is probably not a unique limit for a given sample. In agreement with the previous authors we have estimated from our simulations that, if ξ_{ext} is lower than ~ 100 V/cm, the term containing ξ_{ext} in Eq. (15) can be neglected compared to the other terms. Moreover, for grating periods higher than ~ 0.1 μm it can easily be estimated that B^2 is much smaller than A^2.

To further simplify the denominator, we will assume in the following that the material and the experimental conditions are such that the experiment is performed in the "lifetime regime." According to previous publications[23,24,26,27] this "lifetime regime" is such that the dielectric relaxation time is much shorter than the carriers lifetimes. It means that the dominant terms must be those including a $1/\tau_d$ coefficient. As a consequence, under the preceding conditions (for which we will give more details below), the two terms involving L_n^2 and L_p^2, as well as the lonely K in the third addend of Eq. (15), are all negligible compared to the other terms. Note that these approximations are even better with increasing grating periods. Consequently, DEN transforms into

$$DEN = \frac{\tau_t^2}{\tau_d^2}\left[\begin{array}{c} c_p p_0 \dfrac{\tau_t}{\tau_p}\left(\dfrac{1}{\tau_n} + c_n N_n + c_n N_p\right)(1+X_p) \\ + c_n n_0 \dfrac{\tau_t}{\tau_n}\left(\dfrac{1}{\tau_p} + c_p N_p + c_p N_n\right)(1+X_n) \\ + \mu_n \mu_p K \dfrac{(2+X_n+X_p)}{(\mu_n\tau_n + \mu_p\tau_p)} \end{array}\right]^2 . \tag{17}$$

Introducing an ambipolar mobility-lifetime product as

$$\mu\tau_a = \frac{\mu_n\tau_n \times \mu_p\tau_p}{\mu_n\tau_n + \mu_p\tau_p}, \tag{18}$$

after some lengthy but easy calculations we end with

$$DEN^{1/2} = \frac{q}{\varepsilon\varepsilon_0} G_0 \tau_t \frac{\mu_n\mu_p}{\mu\tau_a}(1+X_n)(1+X_p)\left[\begin{array}{c} 1 + \dfrac{c_p\tau_p}{c_n\tau_n + c_p\tau_p}\dfrac{X_n}{(1+X_p)} + \dfrac{c_n\tau_n}{c_n\tau_n + c_p\tau_p}\dfrac{X_p}{(1+X_n)} \\ + K\mu\tau_a \dfrac{(2+X_n+X_p)}{(1+X_n)(1+X_p)} \end{array}\right]. \tag{19}$$

With the same approximations as those presented in Eq. (11), the numerator of $\Delta j(\Lambda)$ is

$$NUM = -\frac{1}{2}\left(\frac{q}{\varepsilon\varepsilon_0}\right)^2 \Delta G^2\, \xi_{dc}\sigma_0 \tau_t^2 \left(\frac{\mu_n\mu_p}{\mu\tau_a}\right)^2 \left[\frac{\mu_p\tau_p(1+X_n) + \mu_n\tau_n(1+X_p)}{\mu_n\tau_n + \mu_p\tau_p}\right]^2, \tag{20}$$

with $\sigma_0 = q(\mu_n n_0 + \mu_p p_0)$. This leads to the following final expression for $\Delta j(\Lambda)$:

$$\Delta j(\Lambda) = -\frac{1}{2}\left(\frac{\Delta G}{G_0}\right)^2 \frac{\xi_{dc}\sigma_0}{(1+X_n)^2(1+X_p)^2} \frac{\left[\dfrac{\mu_p\tau_p(1+X_n) + \mu_n\tau_n(1+X_p)}{\mu_n\tau_n + \mu_p\tau_p}\right]^2}{\left[1 + \dfrac{c_p\tau_p}{c_n\tau_n + c_p\tau_p}\dfrac{X_n}{(1+X_p)} + \dfrac{c_n\tau_n}{c_n\tau_n + c_p\tau_p}\dfrac{X_p}{(1+X_n)} + K\mu\tau_a\dfrac{(2+X_n+X_p)}{(1+X_n)(1+X_p)}\right]^2} \tag{21}$$

This expression is valid for any type of intrinsic semiconductor in the range of low applied electric fields, low dielectric relaxation time, and a relatively large grating period (see previously). In the following we will concentrate on the case of intrinsic hydrogenated amorphous silicon.

C. Hydrogenated amorphous silicon for large Λ

We will first discuss the respective values of X_n and X_p. From Eq. (12) we have

$$X_n = \tau_n c_n N_n = \frac{c_n n_0 + c_p p_0}{c_p p_0 \int N\, dE} N_n,$$
$$X_p = \tau_p c_p N_p = \frac{c_n n_0 + c_p p_0}{c_n n_0 \int N\, dE} N_p. \tag{22}$$

That means that X_n and X_p are the products of the lifetimes, i.e., capture by all the states in between the quasi-Fermi lev-

els for trapped electrons and holes, by the capture rate of the states k_BT around these levels. Consequently, $X_n<1$ and $X_p<1$ as soon as the quasi-Fermi levels are separated by more than a few k_BT.

Dealing with intrinsic *a*-Si:H means that we can consider $\mu_n\tau_n \gg \mu_p\tau_p$ and, assuming that c_n and c_p are not too different, Eq. (21) transforms into

$$\Delta j(\Lambda) = -\frac{1}{2}\left(\frac{\Delta G}{G_0}\right)^2 \frac{\xi_{dc}\sigma_0}{(1+X_n)^2} \frac{1}{\left[1+K\mu\tau_a\frac{(2+X_n+X_p)}{(1+X_n)(1+X_p)}\right]^2}, \tag{23}$$

where $\mu\tau_a$ can be taken equal to $\mu_p\tau_p$. The coefficient β, defined by Ritter, Zeldov, and Weiser in Ref. 15, can be evaluated by

$$\beta = \frac{j_0+\Delta j(\Lambda)-j_1}{j_0-j_1} = 1-\frac{1}{2}\left(\frac{\Delta G}{G_0}\right)^2 \times \frac{j_0}{(j_0-j_1)(1+X_n)^2} \frac{1}{\left(1+\mu_p\tau_p K\frac{2+X_n+X_p}{(1+X_n)(1+X_p)}\right)^2}, \tag{24}$$

where j_1 is the current density generated by I_1 (i.e., G_1) alone. In the high-Λ limit the term containing K can be neglected, and from Eq. (23) it can be seen that Δj tends towards a constant value,

$$\Delta j(\Lambda \to \infty) = -\frac{1}{2} j_0 \left(\frac{\Delta G}{G_0}\right)^2 \frac{1}{(1+X_n)^2}, \tag{25}$$

while β transforms into

$$\beta_{\text{lim}} = 1-\frac{1}{2}\frac{j_0}{j_0-j_1}\frac{(\Delta G/G_0)^2}{(1+X_n)^2}. \tag{26}$$

Taking into account the power-law dependence of the photoconductivity on the generation rate, $\sigma \propto G^\gamma$, we find that $j_0/(j_0-j_1) \cong 1+G_1/\gamma G_2$, where we recall that G_1 is the generation rate arising from the more intense beam, G_2 is the one coming from the less intense beam, and $G_0=G_1+G_2$. Finally, the following expression can be obtained:

$$N(E_{tn}) = \frac{q\mu_n G_0}{c_n k_B T \sigma_0}\left[\frac{\gamma_0}{(1+G_2/G_1)}\sqrt{\frac{2(1+\gamma G_2/G_1)}{\gamma(1-\beta_{\text{lim}})}}-1\right]. \tag{27}$$

This equation expresses the DOS at the quasi-Fermi energy as a function of material parameters (c_n and μ_n) and experimental magnitudes that can be easily measured (temperature, generation rate, photoconductivity, γ, γ_0, and β_{lim}). The quasi-Fermi energy for trapped electrons E_{tn} can be evaluated from the steady-state photoconductivity σ_0 since, when electrons are the majority carriers, E_{tn} is almost equal to the quasi-Fermi level for free electrons, E_{fn}. The energy position of E_{fn} can be varied either from a temperature scan or a generation rate scan. That gives the basis for a DOS spectroscopy in the upper half of the band gap. The experiment can be performed at a single grating period Λ, provided it is in the high-Λ region where the $\beta(\Lambda)$ curve tends towards a constant value. Thus, the experimental setup is simple.

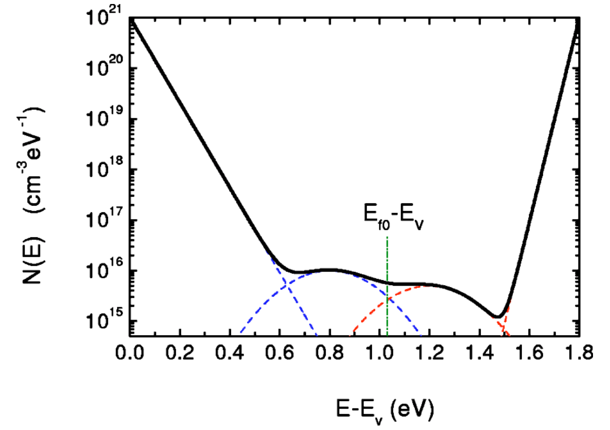

FIG. 1. (Color online) Typical density of states used to calculate the $\beta(\Lambda)$ curves shown in Fig. 2. The position of the Fermi level E_{f0} is indicated.

III. SIMULATIONS

We have performed a numerical simulation of the experiment starting from the DOS shown in Fig. 1, which is quite typical for hydrogenated amorphous silicon. We have taken standard values for the material parameters—such as $c_n=c_p=1\times10^{-8}$ cm^3 s^{-1}, $\mu_n=10$ cm^2 V^{-1} s^{-1}, $\mu_p=1$ cm^2 V^{-1} s^{-1}, equal DOS at the band edges, $N(E_c)=N(E_v)=1\times10^{21}$ cm^{-3} eV^{-1}—and we have solved numerically, *without any approximation*, the set of equations (1) and (3)–(6). The $\beta(\Lambda)$ curve that we get is shown in Fig. 2 (open diamonds), and it closely resembles the typical SSPG experimental curves. We would like to insist on the fact that the DOS that we use here to illustrate the above calculation is one among

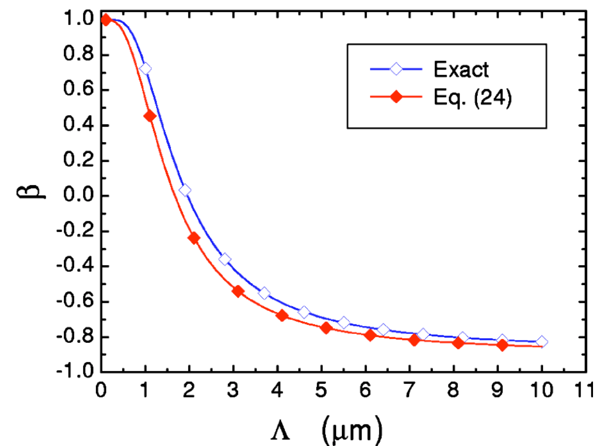

FIG. 2. (Color online) $\beta(\Lambda)$ curves obtained from the exact expression of $\Delta j(\Lambda)$ [Eq. (8), open diamonds] or from the approximate equation (24) (closed diamonds).

many tests that we have made, obtaining always the same typical results. In Fig. 2 we also present a $\beta(\Lambda)$ curve (closed diamonds) calculated from the approximate expression given by Eq. (24). Both curves have been calculated with an external electric field $\xi_{ext}=100$ V/cm, a temperature $T=300$ K, $\gamma_0=1$, and generation rates $G_1=10^{19}$ cm^{-3} s^{-1}, $G_2=G_1/100$. The close agreement between both curves indicates that the approximate expression for β and the complete calculation give similar results. However, we would like to come back to the simplifications that were used to derive Eq. (24). First, we will discuss the various methods proposed in the literature to derive the minority carriers mobility-lifetime product from SSPG data, and we will apply these methods to the results of our simulations. Then, we shall stress the limits of the approximations used in our calculation.

A. Examination of previously-proposed methods to extract information from SSPG data

At this point we would like to discuss the accuracy of the previously-mentioned theoretical descriptions of the SSPG experiment.[22–27] The original formula proposed by RZW in Ref. 16 can be written as

$$\beta = 1 - \frac{2\Phi}{[1+2K(\mu_p\tau_p)_{app}]^2}, \tag{28}$$

where we call $(\mu_p\tau_p)_{app}$ the apparent mobility-lifetime product for holes that would be obtained from a fit of the SSPG data with this formula. A fit of the exact $\beta(\Lambda)$ curve of Fig. 2 with the RZW expression gives $\Phi=0.943$ and $(\mu_p\tau_p)_{app}=7.13\times10^{-9}$ cm^2 V^{-1}. Having solved without any approximation the set of equations (1) and (3)–(6) for steady-state conditions, we know the exact values for these parameters, which are $\Phi=0.948$ and $\mu_p\tau_p=5.84\times10^{-9}$ cm^2 V^{-1}. The parameter Φ is obtained with good accuracy, and that is the common behavior that we have found when the simulations are performed in the region of low applied electric fields. On the other hand, it can be seen that the simple RZW formula overestimates $\mu_p\tau_p$ by 22%, even when we are in the region of low electric fields and in the lifetime regime, where the formula should be valid. The simplified expression for $\beta(\Lambda)$ that we have presented in Eq. (24) indicates that, as X_n and X_p can take values between 0 and 1, the factor $(2+X_n+X_p)/[(1+X_n)(1+X_p)]$ can take values between two (when $X_n=X_p=0$) and one (when $X_n=X_p=1$). For the first case Eq. (24) reduces to the RZW formula, while for the second case Eq. (24) would indicate that the RZW formula overestimates the $\mu_p\tau_p$ product by a factor of two. However, our calculations reveal that other generation rates or other DOS can cause that the RZW formula leads to an overestimation of the exact $\mu_p\tau_p$ product by a factor even larger than two (see below). Thus, the RZW formula should be used with caution, keeping in mind that it probably overestimates the real $\mu_p\tau_p$ value.

In the formulation of Li,[24] a general transport formula is provided for the current under grating conditions [Eq. (48) in Ref. 24] where the ultimate fitting parameters are the drift mobilities μ_n^D and μ_p^D, and the common recombination lifetime τ_R. A fit of the exact $\beta(\Lambda)$ curve (Fig. 2) with Li's Eq. (48) shows a poor sensitivity to the parameter values. If Li's Eq. (52) is used instead (valid in the weak-field condition), the terms can be re-arranged so that the fitting parameters are now L_{amb} and the ratio τ_R/τ_d. A fit of the exact $\beta(\Lambda)$ curve of Fig. 2 with Li's Eq. (52) gives $\tau_R/\tau_d=28$ and $L_{amb}=7.72\times10^{-6}$ cm, which means $\mu_p\tau_p=1.15\times10^{-9}$ cm^2 V^{-1} (a factor of 5 underestimate of the exact $\mu_p\tau_p$) if we approximate $L_{amb}\cong\sqrt{2(k_BT/q)\mu_p\tau_p}$.

Hattori and co-workers[26] propose a quite complicated correction procedure to obtain the true L_{amb} from the apparent L_{app} obtained from the RZW formula. The correction procedure implies knowing the value of the parameter τ_R/τ_d, which according to the authors should be measured by some other technique like modulated photoconductivity or photocurrent decay. Since from the exact solution of the transport equations we know the value of this parameter, we can apply Hattori's correction procedure to get $L_{amb}=1.75\times10^{-5}$ cm, meaning $\mu_p\tau_p=5.92\times10^{-9}$ cm^2 V^{-1}. Thus, although quite cumbersome, Hattori's procedure provides a correct estimation of the true $\mu_p\tau_p$, at least for this generation rate.

In the formulation of Abel and Bauer,[27] the theoretical expression of $\beta(\Lambda,\xi_{ext})$ is expressed as a function of two fitting parameters, $\mu_p\tau_p$ and $\mu_n\tau_d^{rel}$, where τ_d^{rel} is an effective dielectric relaxation time given by $\tau_d^{rel}=(n_0/N_0)\tau_d$, n_0 being the concentration of free electrons and N_0 the total concentration of electrons (free plus trapped), both under uniform illumination. A fit of the exact $\beta(\Lambda)$ curve (Fig. 2) with the Abel–Bauer expression gives $\mu_p\tau_p=6.17\times10^{-9}$ cm^2 V^{-1} and $\mu_n\tau_d^{rel}=1.85\times10^{-9}$ cm^2 V^{-1}, thus providing a good estimation of the correct value with an easy-to-handle formula.

The next step that we have taken was to test the above-described procedures on simulated SSPG curves obtained under different illumination intensities. We performed simulations with the same parameter values that were used to get Fig. 2 except for the generation rate, which was varied in the range $10^{19}\leqslant G_1\leqslant10^{22}$ cm^{-3} s^{-1}, keeping always $G_2=G_1/100$. The results are presented in Fig. 3, where the $\mu_p\tau_p$ values obtained by using the different methods to fit the $\beta(\Lambda)$ curves are plotted as a function of the generation rate. The dependence is characterized by the exponent γ_h, defined as in Ref. 28 by $\mu_p\tau_p\propto G^{(\gamma_h-1)}$. The linear fits (on logarithmic scales) are also presented in Fig. 3, as well as the γ_h values obtained from the different methods, which can be compared to the actual values of $\mu_p\tau_p$ and γ_h calculated from our simulations. As it can be seen, Hattori's method provides the best estimation not only for the $\mu_p\tau_p$ values but also for the γ_h coefficient. At this point we have to add a word of caution on those methods (already mentioned in Sec. I) that use SSPG measurements to get the temperature dependence of the γ_h coefficient, and then perform a fit to this dependence to extract the DOS of the material.[28–30] As can be seen from Fig. 3, the RZW formula is not a reliable means to obtain the γ_h coefficient from SSPG measurements, and what is worse, the accuracy of this formula can even be temperature-dependent. So, in agreement with Hattori *et al.*,[26] we conclude that our results also "contradict a speculation made by Balberg[23] that the SSPG experiments directly measure the correct value of L_{amb} and its light-intensity dependence in the range of conventional light intensities 1–100 mW/cm^2."

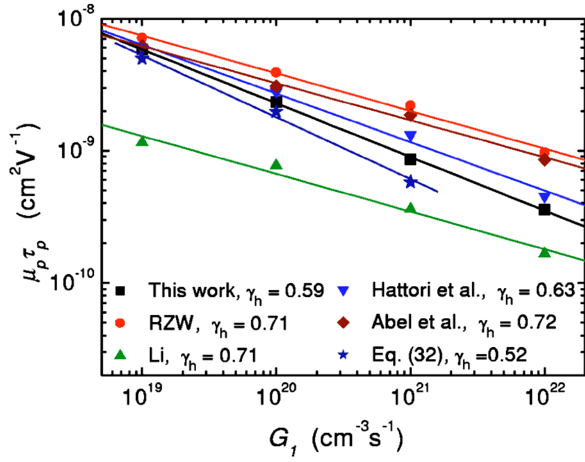

FIG. 3. (Color online) Dependence of $\mu_p\tau_p$ on the generation rate. The "true" $\mu_p\tau_p$ (squares) is obtained from the solution of the transport and charge neutrality equations under steady-state conditions. The other values are obtained from a fit of simulated $\beta(\Lambda)$ curves by using some of the methods proposed in the literature. The $\mu_p\tau_p$ values corrected from the RZW $(\mu_p\tau_p)_{app}$ by means of Eq. (32) are also displayed. The exponent γ_h (see the text for a definition) is obtained from a power-law fit (lines) of the displayed $\mu_p\tau_p$ values.

B. Accuracy of the present calculation

In view of the above results, it could be thought that Eq. (24) would provide a better fit to the SSPG data. However, the presence of three fitting parameters ($\mu_p\tau_p$, X_n, and X_p) leads to poor sensitivity. Moreover, the value of X_p obtained from a fit tends to be negative, suggesting that this formula is not accurate enough. To understand this problem we have to come back to the simplification of the denominator of $\Delta j(\Lambda)$. If we assume that the field-dependent terms are negligible, then *DEN* can be written from Eq. (15) as

$$DEN^{1/2} = \left(\frac{1}{\tau_n\tau_p}\right)\left[\begin{array}{c} c_p p_0 \tau_t (1+X_n+c_n\tau_n N_p)\left(\frac{\tau_t}{\tau_d}(1+X_p)+k^2L_p^2\right) \\ +c_n n_0 \tau_t (1+X_p+c_p\tau_p N_n)\left(\frac{\tau_t}{\tau_d}(1+X_n)+k^2L_n^2\right) \\ +\mu\tau_a K\frac{\tau_t}{\tau_d}(2+X_n+X_p)+k^4L_p^2L_n^2 \end{array}\right] \tag{29}$$

To come to Eq. (17), and eventually to Eq. (24), we have assumed that the dominant terms were those in τ_t/τ_d, an approximation which is *certainly* valid at high Λ but that is wrong for Λ values of the order of ~ 1 μm. For instance, in the present simulation concerning *a*-Si:H for which electrons are the majority carriers, one finds $\tau_t/\tau_d \cong (q/\varepsilon\varepsilon_0)(\mu_n/c_n) \approx 150$ for $\mu_n = 10$ cm^2 V^{-1} s^{-1} and $c_n = 10^{-8}$ cm^3 s^{-1}. Compared to τ_t/τ_d the term $k^2L_p^2$ is almost always negligible, but that is not always the case for the term $k^2L_n^2$. Note that we also have to deal with a term in k^4 that, at this stage, we will assume to be negligible (an assumption that we will justify later). If one keeps the $k^2L_n^2$ term, it adds a new term to Eq. (19), which transforms into

$$DEN^{1/2} = \frac{q}{\varepsilon\varepsilon_0}G_0\tau_t\frac{\mu_n\mu_p}{\mu\tau_a}(1+X_n)(1+X_p)\left[\begin{array}{c} 1+\frac{c_p\tau_p}{c_n\tau_n+c_p\tau_p}\frac{X_n}{(1+X_p)}+\frac{c_n\tau_n}{c_n\tau_n+c_p\tau_p}\frac{X_p}{(1+X_n)} \\ +K\mu\tau_a\frac{(2+X_n+X_p)}{(1+X_n)(1+X_p)}+K\mu_n\tau_n\frac{\varepsilon\varepsilon_0 c_n}{q\mu_n}\left(\frac{1+X_p+c_p\tau_p N_n}{(1+X_n)(1+X_p)}\right) \end{array}\right]. \tag{30}$$

With the usual assumption $\mu_n\tau_n \gg \mu_p\tau_p$ and neglecting the term $c_p\tau_p N_n$ (much smaller than one), a modified Eq. (24) is found such that, by identification with the classical RZW formula, one ends with

$$2(\mu_p\tau_p)_{app} = \mu_p\tau_p\frac{2+X_n+X_p}{(1+X_n)(1+X_p)}+\mu_n\tau_n\frac{\varepsilon\varepsilon_0 c_n}{q\mu_n}\frac{1}{(1+X_n)}. \tag{31}$$

We display in Table I the mobility-lifetime products for electrons and holes obtained from our calculations performed at different G_0 values (the same as Fig. 3). We also present the $(\mu_p\tau_p)_{app}$ values that can be calculated from Eq. (31) taking into account the values of X_n and X_p, and the $(\mu_p\tau_p)_{app}$ values deduced from a "standard" fit of the $\beta(\Lambda)$ curves by means of the RZW method [Eq. (28)]. As can be seen, there is an excellent agreement between the two sets of $(\mu_p\tau_p)_{app}$ values. It can also be shown that assuming $X_n = X_p = 0$ does not largely modify this very good agreement. Therefore, the apparent mobility-lifetime product obtained from a fit of the SSPG data with Eq. (28) can in principle be corrected to give the true value as

$$\mu_p\tau_p \cong (\mu_p\tau_p)_{app} - \frac{\varepsilon\varepsilon_0 c_n}{2q\mu_n}(\mu_n\tau_n). \tag{32}$$

The $\mu_p\tau_p$ values corrected by the application of Eq. (32) are also presented in Table I, where it can be seen that the agreement with the "true" $\mu_p\tau_p$ is quite good except for the largest generation rate. In Fig. 3 we have also presented the $\mu_p\tau_p$ values corrected by Eq. (32). As can be seen, the agreement with the "true" values is rather good except for the highest generation rate, for which the corrected value is too low. This

TABLE I. Evolution with the generation rate of the mobility-lifetime products for electrons and holes. Columns two and three result from the exact solution of the steady-state transport equations. Columns four and five are the apparent mobility-lifetime products for holes that would be obtained by applying the RZW method, either from the classical fit of the $\beta(\Lambda)$ curves with Eq. (28) or from Eq. (31). The last column provides the $\mu_p\tau_p$ values that can be deduced by applying Eq. (32) to the $(\mu_p\tau_p)_{app}$ values of column four.

G_0 ($cm^{-3}\,s^{-1}$)	$\mu_n\tau_n$ (cm^2/V)	$\mu_p\tau_p$	$(\mu_p\tau_p)_{app}$ (Fit)	$(\mu_p\tau_p)_{app}$ [Eq. (31)]	$\mu_p\tau_p$ [Eq. (32)]
1.01×10^{19}	6.40×10^{-7}	5.84×10^{-9}	7.13×10^{-9}	7.20×10^{-9}	5.01×10^{-9}
1.01×10^{20}	5.77×10^{-7}	2.32×10^{-9}	3.90×10^{-9}	3.92×10^{-9}	1.99×10^{-9}
1.01×10^{21}	4.84×10^{-7}	0.86×10^{-9}	2.19×10^{-9}	2.31×10^{-9}	0.58×10^{-9}
1.01×10^{22}	2.90×10^{-7}	0.36×10^{-9}	0.97×10^{-9}	1.23×10^{-9}	5.60×10^{-12}

is due to the fact that, for the highest generation rate, the approximation $X_p\approx 0$ no longer holds. Therefore, Eq. (32) can be applied to improve the initial estimate provided by the RZW method, with some caution for the highest generation rates.

We would like to add a word on the opportunity to define a "lifetime" regime and a "relaxation" regime. The distinction between these two regimes does not appear explicitly in our formulation. Though we have clearly underlined the influence of τ_d, we have shown that the important factor is the ratio τ_t/τ_d, which does not directly involve the carrier lifetime. More work is needed to fully clarify if the distinction between these regimes is really relevant for the SSPG experiment.

Finally, we come back to the term in k^4 that we have neglected in the above discussion. In Hattori's work this term equals $k^4L_{dn}^2L_{dp}^2(\tau_d/\tau')$, while in our work it is equal to $[k^4L_n^2L_p^2/(1+X_n)(1+X_p)](\tau_d/\tau_t)$, both being related to the dielectric relaxation time. Taking $\Lambda=1$ μm and the values from Table I for the mobility-lifetime products, this last term takes values from $\sim$0.15 for the lowest G_0 to $\sim$0.011 for the highest G_0. Both values represent less than a 10% correction to the other terms, so this term in k^4 can be reasonably omitted.

The corrective term that we have included in Eq. (30) also explains why in Fig. 2 the "real" curve is above the $\beta(\Lambda)$ curve calculated from our Eq. (24). This naturally comes from the fact that the term that we have neglected in Eq. (24) is not negligible especially at intermediate Λ. Indeed, $\beta=1-C(\Lambda)$ and $C(\Lambda)$ is higher in Eq. (24) than the true $C(\Lambda)$ because of a smaller denominator leading to a lower β.

C. Determination of the density of states

We have insisted on the accuracy of the present calculation to show that it can be an alternative to those previously developed in the literature. One can see that none of them is perfect, and corrective terms are always necessary to obtain the final and proper value of the ambipolar diffusion length. However, our main aim in this paper is to show that part of the DOS can be deduced from SSPG measurements. Despite the problem of corrective terms, it can be seen from Fig. 2 that the two $\beta(\Lambda)$ curves [exact and obtained from Eq. (24)] are gathering in a single one for large Λ values, since all the terms containing k tend to zero in this region. We are then quite confident on the possibility to deduce the DOS from the $\beta_{\lim}$ measured at high Λ values.

We present in Figs. 4(a) and 4(b) two different DOS' introduced in the simulation with the corresponding reconstructions (SSPG-DOS) obtained from Eq. (27), changing E_{tn} from a variation of T and/or a variation of G_0. The transport parameters were chosen the same as those listed above. As it can be seen, the DOS can be reconstructed with quite good accuracy. We have deliberately chosen to study DOS' with steep variations [narrow deep defect Gaussian distributions, low characteristic temperature of the conduction band tail ($T_c=250$ K)] to show that, despite the DOS roughness, the SSPG-DOS follows rather well the contours of the chosen DOS. With a smoother, and thus less demanding DOS, the SSPG-DOS reconstructions would have been even better. This behavior underlines one of the limits of the method.

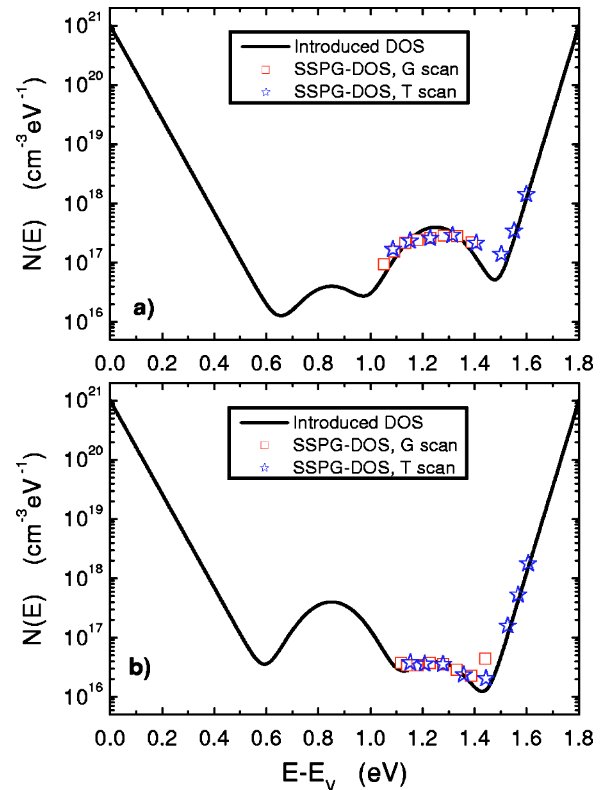

FIG. 4. (Color online) Examples of two different DOS reconstructions by means of Eq. (27).

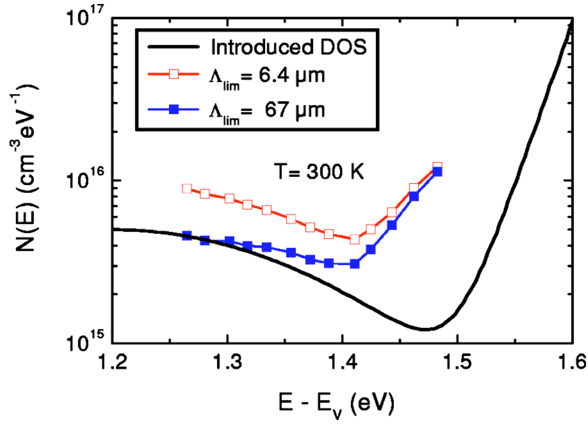

FIG. 5. (Color online) SSPG-DOS reconstruction taking two different values for Λ_{lim}. The simulations giving the $\beta(\Lambda)$ curves, from which the SSPG-DOS has been extracted, were performed with different dc generation rates at T=300 K.

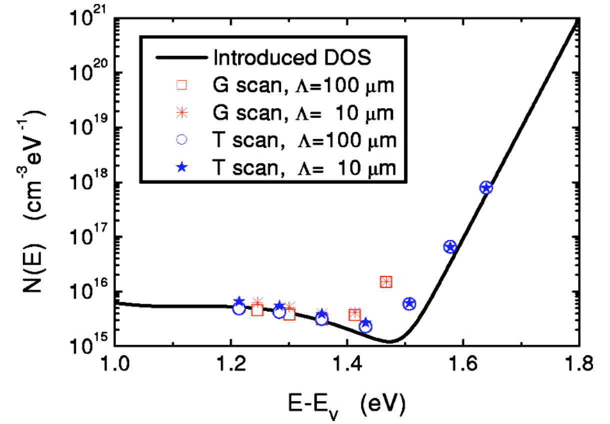

FIG. 6. (Color online) SSPG-DOS reconstruction compared to the introduced DOS in the case of a generation rate scan at a constant T of 300 K, and a temperature scan at a constant G_0 of 10^{19} cm^{-3} s^{-1}. The SSPG-DOS has been calculated for two different Λ_{lim} values.

The limits and accuracy of the method are two points on which we would like to insist. For instance, it is obvious that the grating period Λ_{lim} giving the β_{lim} value is sample-dependent, since it will depends on the $\mu_p\tau_p$ value. We present in Fig. 5 the results that would be obtained applying Eq. (27) to the $\beta(\Lambda)$ curve calculated from the DOS of Fig. 1, taking two different values for Λ_{lim}:6.4 and 64 μm. The simulations have been done with a constant temperature of 300 K and different dc generation rates ranging from 10^{17} to 10^{21} cm^{-3} s^{-1}. Clearly, the choice of Λ_{lim}=6.4 μm does not lead to a good reproduction of the introduced DOS. It can be seen from Fig. 2 that for this value (Λ=6.4 μm) β has not completely reached saturation—a condition that is only reached for Λ larger than 10 μm—thus explaining the discrepancy between the two curves at low $E-E_v$ values. This point brings to light a possible experimental problem, which would be to determine the grating period Λ_{lim} giving the right value for β_{lim}. We can mention, however, that β_{lim} can be easily obtained by measuring a few points in the $\beta(\Lambda)$ curve. Indeed, a fit of the experimental points with the RZW[16] formula [Eq. (28)] will provide β_{lim} from the fitting parameter Φ as β_{lim}=$(1-2\Phi)$.

A different behavior appears for the higher energies, i.e., closer to the conduction band. Both curves deviate from the deep defect density shape to, more or less, parallel the conduction band tail (CBT). This behavior can be explained if we consider the way we introduce N_n [see Eq. (11)] in the calculation of $\beta(\Lambda)$. N_n comes from the evaluation of the integral,

$$Int = \int_{E_v}^{E_c} e_n(E)\tau^2(E)N(E)dE = \int_{E_v}^{E_c} \frac{e_n(E)}{(c_n n_0 + c_p p_0 + e_n(E) + e_p(E))^2} N(E)dE, \quad (33)$$

which, taking into account the fast decrease of $e_p(E)$, can be approximated by

$$Int = \frac{1}{c_n n_0 + c_p p_0}\int_{E_{tp}}^{E_c} \frac{\dfrac{e_n(E)}{c_n n_0 + c_p p_0}}{\left(1+\dfrac{e_n(E)}{c_n n_0 + c_p p_0}\right)^2} N(E)dE = \frac{1}{c_n n_0 + c_p p_0}\int_{E_{tp}}^{E_c} \Theta(E)N(E)dE. \quad (34)$$

The function $\Theta(E)$ is peaked at E_{tn} and decreases exponentially at both sides with a $\pm 1/k_BT$ slope. If the DOS is not varying too fast, then Int can be reasonably taken as Int $=N_n/(c_n n_0+c_p p_0)$, where N_n is truly proportional to $N(E_{tn})$. In this case, the SSPG-DOS follows rather well the true DOS. On the other hand, when E_{tn} gets closer to the conduction band, then the convolution product of the increasing CBT (with a $1/k_BT_c$ slope) and the decreasing part of $\Theta(E)$ (with a $-1/k_BT$ slope) starts to play a non-negligible role in Int. If T is larger than T_c, then the CBT rises more rapidly than $\Theta(E)$ decreases and its contribution to the total N_n can be non-negligible. In that case N_n is no longer proportional to $N(E_{tn})$, and it can be even much larger if the CBT contribution increases. This behavior is also underlined in Fig. 5. The temperature chosen for the simulations has been fixed at 300 K, larger than T_c(=250 K). Increasing the dc generation rate results in a quasi-Fermi level getting closer to the CBT. Since we approximate the integral assuming that the SSPG-DOS is proportional to $N(E_{tn})$, an assumption that turns completely wrong once E_{tn} approaches the CBT, we get too high values for the SSPG-DOS.

As a consequence, the best way to probe the complete DOS would be to choose G_0 and T so that, when E_{tn} approaches the CBT, the sample temperature is lower than the conduction band tail characteristic temperature. This is illustrated in Fig. 6. The simulation has been performed with the DOS of Fig. 1 and the parameters listed above. First, it can be seen that the SSPG-DOS reconstructions from Eq. (27) using two different Λ_{lim} (10 and 100 μm) give almost the

same data points, showing that, for this peculiar "sample," the choice of $\Lambda_{\text{lim}}=10\ \mu$m is convenient. Second, as in the case shown in Fig. 5, the SSPG-DOS reconstructions calculated at room temperature with G_0 varying from 10^{17} to 10^{21} cm^{-3} s^{-1} deviate from the true DOS at high G_0 values, i.e., when E_{tn} gets closer to the conduction band. This problem disappears when the β curves are calculated with a mean G_0 value of 10^{19} cm^{-3} s^{-1} and the temperature is varied in the range 100–400 K. With this low generation rate the quasi-Fermi level for trapped electrons enters the CBT only at low temperatures, when $1/k_BT \gg 1/k_BT_c$, being therefore the $\Theta(E)$ function extremely narrow compared to the CBT width. It can be seen in Fig. 6 that this procedure results in an excellent reconstruction of the introduced DOS by the SSPG-DOS.

IV. EXPERIMENTAL

To prove the experimental usefulness of the technique, measurements on two hydrogenated amorphous silicon samples have been performed. Note that, according to Eq. (27), we do not obtain directly the true density of states from the experimental data, but rather the quantity $N(E_{tn}) \times c_n/\mu_n$. It is exactly this quantity that is obtained from the modulated photocurrent (MPC) technique. Thus, the validity of the SSPG-DOS determination can be confirmed by comparing it to the MPC-DOS obtained on the same a-Si:H sample by using the same standard values for c_n and μ_n.

We have applied the new technique to two standard hydrogenated amorphous silicon samples, prepared under conditions described elsewhere.[33] Sample 1 has a thickness of 0.65 μm, a room-temperature dark conductivity of $6.5 \times 10^{-8}\ \Omega^{-1}$ cm^{-1}, and an activation energy of 0.62 eV; while Sample 2 has a thickness of 1.1 μm, a room-temperature dark conductivity of $2.7 \times 10^{-9}\ \Omega^{-1}$ cm^{-1}, and an activation energy of 0.69 eV. Two aluminum coplanar electrodes, with a gap of 0.5 mm, have been evaporated on the samples. A He-Ne laser providing a light intensity at the sample surface of 90 mW/cm^2 has been used as a source of coherent illumination. An intensity ratio $I_1/I_2=85$ has been used, and the less intense beam has been chopped at a frequency of 111 Hz to perform SSPG measurements. Assuming that the RZW formula provides a good estimation of the Φ factor (see Sec. III A), after measuring γ and taking into account that $\Phi = \gamma\gamma_0^2$ (Ref. 16), the grating quality factor γ_0 was found to be close to one for our SSPG setup and for these samples. Then we have fixed $\Lambda_{\text{lim}}=10\ \mu$m and we have measured the coefficients β and γ as a function of the temperature and generation rate. Measurements have been performed under vacuum, with a pressure lower than 10^{-5} Torr. For both samples we performed a temperature scan from 100 to 370 K in 30 K steps at a fixed generation rate of 2×10^{21} cm^{-3} s^{-1}; while for Sample 2 we also changed the generation rate between 2×10^{21} cm^{-3} s$^{-1} > G_0 > 2\times10^{19}$ cm^{-3} s^{-1} at a fixed temperature of 370 K. The results of the application of Eq. (27) to the measured data are shown in Figs. 7(a) and 7(b), where our new technique based on SSPG measurements is compared with the MPC methods, performed both in the high frequency[10] (HF-MPC) and the low frequency[11] (LF-MPC) limits. To obtain absolute DOS values, an electron mobility $\mu_n=10$ cm^2 V^{-1} s^{-1} and a capture coefficient $c_n = 10^{-8}$ cm^3 s^{-1} have been assumed in all the methods. To set the energy scale we have used $E_{tn} \approx E_{fn} = E_c - k_BT \ln[q\mu_n k_BTN(E_c)/\sigma_0]$ for SSPG and LF-MPC (see Ref. 11), and $E_{\omega n} = E_c - k_BT \ln[c_n k_BTN(E_c)/\omega]$ for HF-MPC (see Ref. 10), where the pulsation of the excitation was varied in the range 10^2 s$^{-1} \leqslant \omega \leqslant 6\times10^5$ s^{-1}. Note that energies are now referred to the conduction band edge to avoid uncertainties in the value of the mobility gap for these samples. In Fig. 7(a) it can be appreciated that for Sample 1 the agreement among the three methods is very good over the energy range where they overlap. For the HF-MPC method, each curve corresponds to a frequency scan performed at a different temperature. As demonstrated in Ref. 10, the actual DOS is reproduced by the upper envelope of all the frequency scans performed at different temperatures. The maxima exhibited by the curves at low temperatures (low energies) are due to a bad signal to noise ratio appearing at high frequencies, i.e., when the DOS is high and the sample response is proportionally low. The departure of the curves from the upper envelope at high temperatures (high energies) results from the influence of the continuous flux used in the method. For a detailed discussion of the HF-MPC method, and in particular on the DOS shape determination, the reader is referred to

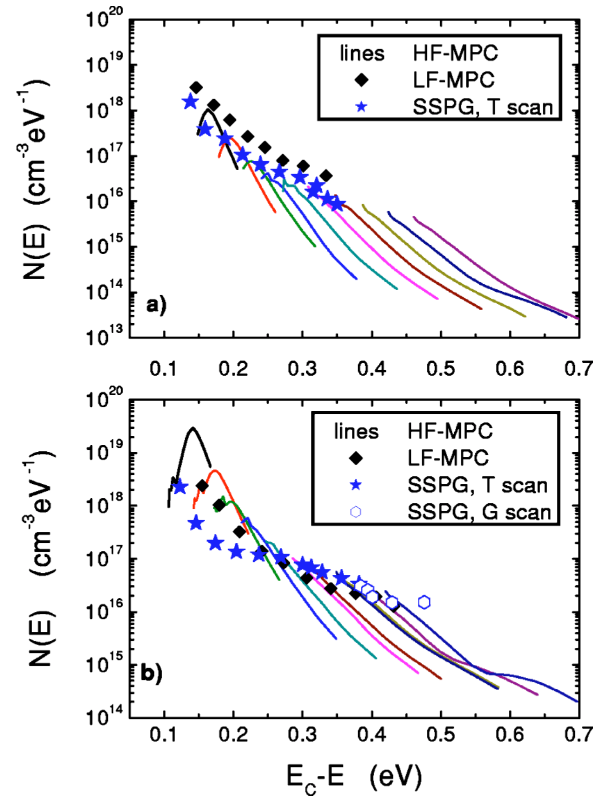

FIG. 7. (Color online) A comparison between DOS determinations for Sample 1 (a) and Sample 2 (b) from modulated photoconductivity in the low frequency (LF-MPC) and high frequency (HF-MPC) domains, and from SSPG as a function of temperature (a) and as a function of temperature and generation rate (b). $N(E_c) = 10^{21}$ cm^{-3} eV^{-1}, $\mu_n=10$ cm^2 V^{-1} s^{-1}, and $c_n=10^{-8}$ cm^3 s^{-1} have been assumed in all cases.

Ref. 10. A fit of the band-tail region with an exponential function gives a characteristic energy of 23±2 meV, meaning a characteristic temperature of 270 K, in agreement with previous determinations.[34] It can be seen that the HF-MPC provides the DOS over the largest energy range. However, the range of the SSPG-DOS determination can be enlarged if the temperature as well as the generation rate are varied simultaneously, as shown in Fig. 7(b) for Sample 2. From this latter figure it can be seen that the agreement among the three methods is very good except for energies close to the conduction band-tail. A fit of the band-tail DOS with an exponential function gives characteristic energies of 20, 26, and 29 meV from SSPG, LF-MPC, and HF-MPC, respectively. The disagreement in this region may be due to a failure of the simplifying hypotheses of the different methods when the DOS is steeper than $k_B T$, as discussed in Sec. III C of this work, Sec. IV B of Ref. 10, and Sec. III B of Ref. 11. Another possible source of discrepancies may be the fact that the developments made for the different methods are mainly valid for a single type of states. More work is needed to overlook the influence on the DOS evaluation of the presence of different types of states in the gap. However, the general agreement between the three DOS estimates in both figures means that this new technique provides a simple method for DOS determinations, with an accuracy at least comparable to the one of the MPC techniques.

V. CONCLUSION

In conclusion, we have described a novel and accurate method based on SSPG measurements in the high-Λ limit to determine the DOS of intrinsic semiconductors. We have presented the basic equations describing the phenomenon, and we have solved them to obtain a simple formula relating the DOS at the electron quasi-Fermi level to SSPG measurements. Contrary to previous approaches, the DOS is not obtained from a fit of measured SSPG data. Instead, the measured values are used to directly reconstruct the DOS of the sample. This new method has been tested taking the case of a-Si:H as an example. First, we have performed simulations starting from a typical DOS for a-Si:H. We have examined previous theoretical descriptions of the SSPG phenomenon, providing the $\mu_p \tau_p$ values that would be obtained by applying the previously-proposed methods to SSPG data obtained at different G_0 values. We have studied the accuracy of our approximate formulas to reproduce the SSPG curves, and we have proposed a corrective term to obtain the $\mu_p \tau_p$ value from the $(\mu_p \tau_p)_{app}$ that arises from a fit of the data with the RZW formula. We have also studied the accuracy and limitations of our method to reproduce an introduced DOS. Finally, we have presented experimental measurements on two a-Si:H samples showing that the method is applicable, experimentally simple, and capable of providing DOS determinations compatible with the ones obtained from the modulated photoconductivity methods.

ACKNOWLEDGMENTS

This work was supported by project PEI N° 6329 from CONICET and project A02E01 from Ecos Sud-SECyT. One of the authors (J. A. S.) acknowledges support from the Alexander von Humboldt Foundation.

[1] W. E. Spear and P. G. LeComber, J. Non-Cryst. Solids **8–10**, 727 (1972).
[2] I. Solomon, R. Benferhat, and H. Tran-Quoc, Phys. Rev. B **30**, 3422 (1984).
[3] P. Viktorovitch, J. Appl. Phys. **52**, 1392 (1981).
[4] G. F. Seynhaeve, R. P. Barclay, G. J. Adriaenssens, and J. M. Marshall, Phys. Rev. B **39**, 10 196 (1989).
[5] W. B. Jackson, S. M. Kelso, C. C. Tsai, J. W. Allen, and S.-J. Oh, Phys. Rev. B **31**, 5187 (1985).
[6] W. E. Spear, J. Non-Cryst. Solids **1**, 197 (1969).
[7] M. Vanecek, J. Kocka, J. Stuchlík, and A. Tríska, Solid State Commun. **39**, 1199 (1981).
[8] R. A. Street and A. D. Yoffe, Thin Solid Films **11**, 161 (1972).
[9] J. A. Schmidt, R. R. Koropecki, R. Arce, A. Dussan, and R. H. Buitrago, J. Non-Cryst. Solids **338–340**, 322 (2004).
[10] C. Longeaud and J. P. Kleider, Phys. Rev. B **45**, 11 672 (1992).
[11] R. R. Koropecki, J. A. Schmidt, and R. Arce, J. Appl. Phys. **91**, 9865 (2002).
[12] F. Wang and R. Schwarz, Phys. Rev. B **52**, 14 586 (1995).
[13] M. Q. Tran, Philos. Mag. B **72**, 35 (1995).
[14] J. A. Schmidt and C. Longeaud, Appl. Phys. Lett. **85**, 4412 (2004).
[15] D. Ritter, E. Zeldov, and K. Weiser, Appl. Phys. Lett. **49**, 791 (1986).
[16] D. Ritter, K. Weiser, and E. Zeldov, J. Appl. Phys. **62**, 4563 (1987).
[17] G. H. Bauer, C. E. Nebel, and H.-D. Mohring, Mater. Res. Soc. Symp. Proc. **118**, 679 (1988).
[18] L. Yang, A. Catalano, R. R. Arya, and I. Balberg, Appl. Phys. Lett. **57**, 908 (1990).
[19] M. Goerlitzer, N. Beck, P. Torres, J. Meier, N. Wyrsch, and A. Shah, J. Appl. Phys. **80**, 5111 (1996).
[20] R. Brüggemann, Appl. Phys. Lett. **73**, 499 (1998).
[21] J. Y. Duboz, F. Binet, D. Dolfi, N. Laurent, F. Scholz, J. Off, A. Sohmer, O. Briot, and B. Gil, Mater. Sci. Eng., B **50**, 289 (1997).
[22] D. Ritter, E. Zeldov, and K. Weiser, Phys. Rev. B **38**, 8296 (1988).
[23] I. Balberg, J. Appl. Phys. **67**, 6329 (1990).
[24] Y.-M. Li, Phys. Rev. B **42**, 9025 (1990).
[25] I. Balberg, Phys. Rev. B **44**, 1628 (1991).
[26] K. Hattori, H. Okamoto, and Y. Hamakawa, Phys. Rev. B **45**, 1126 (1992).
[27] C.-D. Abel and G. H. Bauer, in *Amorphous Silicon Technology*, MRS Symposia Proceedings No. 258 (Materials Research Society, Pittsburgh, 1992), p. 705; C.-D. Abel and G. H. Bauer, Prog. Photovoltaics **1**, 269 (1993); C.-D. Abel, G. H. Bauer, and W. H. Bloss, Philos. Mag. B **72**, 551 (1995).

[28] I. Balberg, R. Nidis, L. F. Fonseca, S. Z. Weisz, J. P. Conde, P. Alpuim, and V. Chu, Phys. Rev. B **63**, 113201 (2001).
[29] I. Balberg, J. Non-Cryst. Solids **299–302**, 531 (2002).
[30] I. Balberg, Y. Dover, R. Naides, J. P. Conde, and V. Chu, Phys. Rev. B **69**, 035203 (2004).
[31] J. P. Nicholson, Appl. Phys. Lett. **77**, 2563 (2000).
[32] J. G. Taylor and G. W. Simmons, J. Non-Cryst. Solids **8–10**, 940 (1972).
[33] R. H. Buitrago, R. Arce, and R. R. Koropecki, J. Non-Cryst. Solids **164–166**, 259 (1993).
[34] See, for example, R. A. Street, *Hydrogenated Amorphous Silicon* (Cambridge University Press, Cambridge, 1991), p. 81.